

# Photochemistry of forbidden oxygen lines in the inner coma of 67P/Churyumov-Gerasimenko

G. Cessateur,<sup>1</sup> J. De Keyser,<sup>1,2</sup> R. Maggiolo,<sup>1</sup> A. Gibbons,<sup>1,3</sup> G. Gronoff,<sup>4</sup> H. Gunell,<sup>1</sup> F. Dhooghe,<sup>1</sup> J. Loreau,<sup>3</sup> N. Vaeck,<sup>3</sup> K. Altwegg,<sup>5,6</sup> A. Bieler,<sup>5,7</sup> C. Briois,<sup>8</sup> U. Calmonte,<sup>5</sup> M. R. Combi,<sup>7</sup> B. Fiethe,<sup>9</sup> S. A. Fuselier,<sup>10,11</sup> T. I. Gombosi,<sup>7</sup> M. Hässig,<sup>5,10</sup> L. Le Roy,<sup>5</sup> E. Neefs,<sup>12</sup> M. Rubin<sup>5</sup>, and T. Sémon<sup>5</sup>

---

<sup>1</sup>Space Physics Division, Belgian Institute

for Space Aeronomy, Ringlaan 3, B-1180

Brussels, Belgium

<sup>2</sup>Center for Plasma Astrophysics,

Katholieke Universiteit Leuven,

Celestijnenlaan 200B, B-3001 Heverlee,

Belgium

<sup>3</sup>Service de Chimie Quantique et

Photophysique, Université Libre de

Bruxelles (ULB), Av. F. D. Roosevelt 50,

B-1050 Brussels, Belgium

<sup>4</sup>Science Directorate, Chemistry and

Dynamics Branch, NASA Langley Research

**This is the author manuscript accepted for publication and has undergone full peer review but has not been through the copyediting, typesetting, pagination and proofreading process, which may lead to differences between this version and the Version of Record. Please cite this article as doi:**

10.1029/2015JA022013

December 26, 2015, 3:30pm

D R A F T

Center, Hampton, Virginia USA; SSAI,  
Hampton, Virginia USA

<sup>5</sup>Physikalisches Institut, University of  
Bern, Sidlerstr. 5, CH-3012 Bern,  
Switzerland

<sup>6</sup>Center for Space and Habitability,  
University of Bern, Sidlerstr. 5, CH-3012  
Bern, Switzerland

<sup>7</sup>Department of Climate and Space  
Sciences and Engineering, University of  
Michigan, 2455 Hayward, Ann Arbor, MI  
48109, USA

<sup>8</sup>Laboratoire de Physique et Chimie de  
l'Environnement et de l'Espace (LPC2E),  
UMR 7328 CNRS Université d'Orléans,  
France

<sup>9</sup>Institute of Computer and Network  
Engineering (IDA), TU Braunschweig,  
Hans-Sommer-Strae 66, D-38106  
Braunschweig, Germany

**Key Points.**

- The presence of O<sub>2</sub> within 67P's atmosphere increases significantly the red line emission.
- Estimations of CO<sub>2</sub> abundances based on the G/R ratio should be revised due to the O<sub>2</sub> presence.
- Space weather phenomena such as solar flares have an impact on the comet photochemistry.

**Abstract.**

Observations of the green and red-doublet emission lines have previously been realized for several comets. We present here a chemistry-emission coupled model to study the production and loss mechanisms of the O(<sup>1</sup>S) and O(<sup>1</sup>D) states, which are responsible for the emission lines of interest, for comet 67P/Churyumov-Gerasimenko. The recent discovery of O<sub>2</sub> in significant abun-

---

<sup>10</sup>Space Science Division, Southwest

Research Institute, 6220 Culebra Road, San  
Antonio, Texas, 78228, USA

<sup>11</sup>Department of Physics and Astronomy,  
University of Texas at San Antonio, San  
Antonio, Texas, USA

<sup>12</sup>Engineering Division, Belgian Institute  
for Space Aeronomy, Ringlaan 3, B-1180,  
Brussels, Belgium

dance relative to water ( $3.7 \pm 1.5$  %) within the coma of 67P has been taken into consideration for the first time in such models. We evaluate the effect of the presence of  $O_2$  on the green to red-doublet emission intensity ratio, which is traditionally used to assess the  $CO_2$  abundance within cometary atmospheres. Model simulations, solving the continuity equation with transport, show that not taking  $O_2$  into account leads to an underestimation of the  $CO_2$  abundance within 67P, with a relative error of about 25 %. This strongly suggests that the green to red-doublet emission intensity ratio alone is not a proper tool for determining the  $CO_2$  abundance, as previously suggested. Indeed, there is no compelling reason why  $O_2$  would not be a common cometary volatile, making revision of earlier assessments regarding the  $CO_2$  abundance in cometary atmospheres necessary. The large uncertainties of the  $CO_2$  photodissociation cross section imply that more studies are required in order to better constrain the  $O(^1S)$  and  $O(^1D)$  production through this mechanism. Space weather phenomena, such as powerful solar flares, could be used as tools for doing so, providing additional information on a good estimation of the  $O_2$  abundance within cometary atmospheres.

## 1. Introduction

1 Comets are physicochemical witnesses of the conditions of the early solar system and  
2 their study can bring us valuable information concerning solar system formation theories.  
3 Comet researchers usually have to resort to remote observations. Numerous studies have  
4 been devoted to the direct observation of atomic oxygen lines [*Morghenthaler et al.*, 2007;  
5 *Cochran*, 2008; *McKay et al.*, 2015]. Photodissociation of H<sub>2</sub>O, CO<sub>2</sub>, and CO result in  
6 the release of an oxygen atom in an excited state, either O(<sup>1</sup>D) or O(<sup>1</sup>S). The emission  
7 lines of interest are the radiative transition from O(<sup>1</sup>D) to O(<sup>3</sup>P), which is responsible for  
8 the formation of the double red line emission at 630 and 636.4 nm and the deactivation  
9 of the O(<sup>1</sup>S) state leading to the green line emission at 557.7 nm. In that regard, the  
10 CO<sub>2</sub> abundance relative to the H<sub>2</sub>O abundance has been previously inferred from remote  
11 sensing data by taking the ratio between the intensities of the excited atomic oxygen green  
12 and red-doublet emission lines in comets (hereafter G/R ratio) [*McKay et al.*, 2012, 2013;  
13 *Decock et al.*, 2013, 2015]. Up until now, the photodissociation of other major volatiles  
14 such as water, carbon dioxide, the hydroxyl radical, and carbon monoxide have been  
15 considered as the main processes for producing O(<sup>1</sup>S) and O(<sup>1</sup>D) atoms [see e.g. *Bhardwaj*  
16 *and Raghuram*, 2012, and references therein].

17 The Double Focusing Mass Spectrometer (DFMS), part of the Rosetta Orbiter Sensor  
18 for Ion and Neutral Analysis (ROSINA), onboard the Rosetta spacecraft, is a high resolu-  
19 tion mass spectrometer allowing the precise analysis of the cometary exosphere (or coma)  
20 of comet 67P/Churyumov-Gerasimenko (hereafter 67P) [*Balsiger et al.*, 2007]. DFMS has  
21 already delivered several important results, for instance the D/H ratio in water in 67P

22 [Altwegg *et al.*, 2015], the discovery of N<sub>2</sub> [Rubin *et al.*, 2015] and O<sub>2</sub> [Bieler *et al.*, 2015].  
23 Even though the Rosetta mission is a unique opportunity to study one comet up-close,  
24 the results it delivers are likely to be applicable to other comets as well. For instance, the  
25 detection of O<sub>2</sub> has been possible in 67P thanks to in situ mass spectrometry with the  
26 very high mass resolution and sensitivity of DFMS. Since there is no compelling reason  
27 to consider 67P unique, this would suggest that molecular oxygen is also present in other  
28 cometary atmospheres. This molecule has never been considered in coupled chemistry-  
29 emission models determining the G/R ratio. However, the photodissociation of O<sub>2</sub> is also  
30 an important source of O(<sup>1</sup>S) and O(<sup>1</sup>D), and should therefore be taken into account. The  
31 goal of this paper is first to assess the impact of previously undetected molecules such  
32 as O<sub>2</sub> on the production of excited oxygen states O(<sup>1</sup>S) and O(<sup>1</sup>D), and on the O(<sup>1</sup>S)  
33 to O(<sup>1</sup>D) ratio as a function of the cometocentric distance. We furthermore discuss the  
34 implication of the presence of O<sub>2</sub> on previous cometary models and observations. Finally,  
35 we explore the impact of the CO<sub>2</sub> cross section uncertainties on the G/R ratio as well as  
36 the impact of the solar UV flux within a planetary space weather context.

## 2. Chemistry-emission coupled model

37 The purpose of this section is to describe the chemistry-emission coupled model for  
38 67P. We use the spherically-symmetric expansion model of *Haser* [1957] to estimate the  
39 number densities  $n_i(r)$  of the  $i$ th parent species at a cometocentric distance  $r$  from the  
40 nucleus. The water production rate from the surface of 67P near perihelion has been  
41 estimated at  $4 \times 10^{27} \text{s}^{-1}$  for July 2015, while the velocity of the escaping volatiles has been  
42 measured to be  $700 \text{ m s}^{-1}$  using the data of the COmet Pressure Sensor (COPS), part

of the ROSINA experiment. We consider the primary volatile elements detected by the ROSINA/DFMS spectrometer, H<sub>2</sub>O, CO<sub>2</sub>, CO, and O<sub>2</sub>.

The average CO and CO<sub>2</sub> abundances relative to water have been estimated at 25 % and 8.3 % for the month of July 2015. Those abundances are in bulk agreement with the values presented by *Hässig et al.* [2015]; *Le Roy et al.* [2015]. The detection of O<sub>2</sub>, as discussed by *Bieler et al.* [2015], will have an impact on the production rate of the atomic states O(<sup>1</sup>D) and O(<sup>1</sup>S). The ROSINA/DFMS instrument onboard Rosetta has indeed detected the presence of O<sub>2</sub> in high quantity, with an abundance relative to water of  $3.7 \pm 1.5$  %, which puts this volatile in an abundance range comparable to that of CO<sub>2</sub>. An average O<sub>2</sub> abundance of 4 %, as measured in July 2015, will be considered in the following. The resulting neutral atmosphere is displayed in Figure 1.

## 2.1. Production reactions

The dominant source of the production of O(<sup>1</sup>D) and O(<sup>1</sup>S) in the inner coma ( $\leq 10^4$  km) is the photodissociation of the major oxygen-bearing volatile components [see e.g. *Decock et al.*, 2015]. A simple model for evaluating the green and red-doublet line emissions within 67P's atmosphere as a function of the nucleocentric distance is presented here. We consider only the impact of the solar UV flux on the production of the three forbidden oxygen lines of interest. The photoelectron impact dissociative excitation of volatile components was shown to make only a minor contribution ( $\leq 1\%$ ) in the inner coma [see e.g. *Bhardwaj and Raghuram*, 2012]. The ion-recombination reactions and photodissociation of hydroxyl also have a minor contribution to the production of O(<sup>1</sup>D) and O(<sup>1</sup>S) in the inner coma. We consider a heliocentric distance of about 1.35 AU for 67P, corresponding to its position in the solar system in July 2015 not far from perihelion. A composite solar spectrum from 1

to 300 nm with 1-nm bin resolution is used, scaled to a heliocentric distance of 1.35 AU using an inverse distance-squared law, based on the observations of three instruments in Earth orbit. Data in the 1-27 nm range comes from the *XUV Photometer System* [XPS, Woods et al., 2008] onboard the *SOLar Radiation and Climate Experiment* (SORCE, Rottman [2005]). The 27-115 nm range data is taken from the *Solar Extreme Ultraviolet Experiment* (SEE) onboard TIMED [Woods et al., 2005]. Finally the spectral range 115-300 nm comes from the *SOLar Stellar Irradiance Comparison Experiment* [SOLSTICE, McClintock et al., 2005], also onboard the SORCE spacecraft. The composite solar UV spectrum is displayed in Figure 2 (black curve), and the corresponding level of solar activity in terms of the F10.7 index is about 104 for July 2015.

In order to take account for the attenuation of solar radiation by the cometary atmosphere at wavelength  $\lambda$  and altitude  $z$ , a Beer-Lambert law is considered:

$$F(\lambda, z) = F_{\infty}(\lambda)e^{-\tau_{tot}(z, \lambda)}, \quad (1)$$

where  $F_{\infty}(\lambda)$  is the solar UV flux at the top of the cometary atmosphere, taken at  $10^4$  km from the nucleus. We use a grid with adaptive mesh size ranging from 1 km close to the surface to 10 km far from the comet. The solar UV flux at each altitude  $z$  from the nucleus is computed taking into account the wavelength-dependent total photoabsorption cross section for the different neutral species, used for computing the optical depth  $\tau(z)_{tot}$ . The different total cross sections relative to water, carbon monoxide, carbon dioxide, and molecular oxygen are taken from the PHIDRATES database (see <http://phidrates.space.swri.edu/>) which is based on the work of Huebner and Mukherjee [2015]. The solar UV flux is mostly absorbed in the spectral range between 60 and 100



86 nm with an absorption average of about 12.5 % between the top of the atmosphere and  
 87 at 10 km above the comet, with a maximum at 90 nm with 17 % of absorbed flux. Above  
 88 100 nm, the solar UV flux is mostly absorbed until 130 nm mainly because of the presence  
 89 of water and O<sub>2</sub> with an average absorption of about 5 %.

90 The production rates coefficients for an atomic state  $a$ , i.e. O(<sup>1</sup>D) or O(<sup>1</sup>S) from the  
 91 photodissociation of the considered species  $i$ , i.e water, carbon dioxide, molecular oxygen,  
 92 and carbon monoxide, are computed using the following equation:

$$k^a(z) = \int_{\lambda} \sigma_a^i(\lambda) F(\lambda, z) d\lambda \quad (2)$$

93 where  $\sigma_a^i(\lambda)$ , are the partial cross sections leading to the photoproduction of the atomic  
 94 states O(<sup>1</sup>D) and O(<sup>1</sup>S), also taken from the PHIDRATES database for water, carbon  
 95 dioxide, and carbon monoxide. There is still, however, an ongoing discussion regarding the  
 96 O(<sup>1</sup>S) production through the photodissociation of water. For the sake of comparison, we  
 97 follow here the approach used by *Bhardwaj and Raghuram* [2012], assuming a 0.5% yield  
 98 at 121.6 nm. Regarding the production of O(<sup>1</sup>S) from CO<sub>2</sub>, the considered partial cross  
 99 section is obtained by multiplying the total cross section of CO<sub>2</sub> by the yield recommended  
 100 by *Huestis et al.* [2010]. Regarding the production of O(<sup>1</sup>S) from the photodissociation  
 101 of CO, we also follow the approach from *Bhardwaj and Raghuram* [2012] since no partial  
 102 cross section data is available in the PHIDRATES database. The computed production  
 103 rate coefficients at the top of the cometary atmosphere are summarised in Table 1, for  
 104 a heliocentric distance of 1.35 AU. With the number densities prevailing in 67P's atmo-  
 105 sphere, the solar flux is attenuated in such a way that there is a difference of about 2.7-3%  
 106 between the production rate coefficients from water at the top of the atmosphere com-

pared to 10 km altitude. The solar UV flux is more absorbed for wavelengths between 70-90 nm, leading to a more pronounced decrease of the production rates from CO<sub>2</sub> and CO of about 8% and 12%, respectively.

The presence of O<sub>2</sub> is taken into account here for the first time in such modeling. The photodissociation of O<sub>2</sub> follows three principal channels for the wavelengths of interest. Above 177 nm, only the O(<sup>3</sup>P) ground state is produced. For the wavelength range from 115 nm to 177 nm, the photoproducts are O(<sup>1</sup>D) and O(<sup>3</sup>P) and the production yield is taken from *Lee et al.* [1977]. Below 115 nm down to 90 nm, photodissociation results in O(<sup>1</sup>S) and O(<sup>3</sup>P), and the recommended cross section from the ATMOCIAAD database is used [*Gronoff et al.*, 2011]. This set of cross section, available upon request, has been widely used within an aeronomic context for modeling the Mars airglow [*Gronoff et al.*, 2012a, b], in a cometary studies context for the comet Siding Spring [*Gronoff et al.*, 2014] and more recently used for retrieving carbon dioxide and molecular nitrogen for the upper atmosphere of Mars using the Imaging Ultraviolet Spectrograph (IUVS) on board NASA's Mars Atmosphere and Volatile Evolution (MAVEN) spacecraft [*Evans et al.*, 2015]. At a distance of 1.35 AU and for a solar flux corresponding to a solar activity of F10.7 = 104, the computed reaction rates at the top of the atmosphere are  $1.46 \times 10^{-6} \text{ s}^{-1}$  and  $4.5 \times 10^{-9} \text{ s}^{-1}$  for the photoproduction of O(<sup>1</sup>D) and O(<sup>1</sup>S), respectively. The attenuation of the solar UV flux in this case leads, respectively, to a 1.21% and 8.92% decrease.

The calculated O(<sup>1</sup>D) and O(<sup>1</sup>S) production rate profiles are presented in Figure 3. The major source of O(<sup>1</sup>D) in the inner coma is clearly the photodissociation of water, with a production rate of  $2 \times 10^3 \text{ cm}^{-3} \text{ s}^{-1}$  at 10 km from the nucleus. A secondary contribution comes from the photodissociation of CO<sub>2</sub>, but represents only 10 % of the total produced

130 O(<sup>1</sup>D). The photodissociation of O<sub>2</sub> plays also a minor role compared to water, but is as  
131 large as the contribution of CO<sub>2</sub>, and represents 10 % of the total O(<sup>1</sup>D) production. The  
132 photodissociation of CO is clearly a minor process, representing roughly 1 % of the total.  
133 The radiative decay of O(<sup>1</sup>S) leads also to the production of O(<sup>1</sup>D), through reaction 9  
134 in Table 2. As discussed in Section 2.2, this is an effective process with a contribution  
135 equivalent to the photodissociation of CO<sub>2</sub> and O<sub>2</sub> producing atomic oxygen O(<sup>1</sup>D).

136 Both the photodissociation of water and CO<sub>2</sub> are important O(<sup>1</sup>S) sources for 67P.  
137 Indeed, the number density of CO<sub>2</sub> is high enough to play a major role along with water.  
138 This has already been modeled for comets with similar atmospheric compositions [see  
139 e.g. comets C/2003 K4 (LINEAR) and 116P/Wild 4 as discussed by *Raghuram and*  
140 *Bhardwaj*, 2014]. The total production of O(<sup>1</sup>S) close to the nucleus at 10 km is about  
141  $2 \times 10^2 \text{ cm}^{-3} \text{ s}^{-1}$ . The photodissociation of CO leading to O(<sup>1</sup>S) is a secondary process  
142 with a contribution of 10 %. The photodissociation of O<sub>2</sub> plays only a minor role, with  
143 less than 1 % of the total produced O(<sup>1</sup>S).

144 We also looked which parts of the solar UV flux influence the production of O(<sup>1</sup>D)  
145 and O(<sup>1</sup>S). When considering the neutral densities presented in Figure 1, the solar UV  
146 at Lyman  $\alpha$  is responsible for 70 % of the production of O(<sup>1</sup>D), coming mainly from the  
147 photodissociation of water. The following spectral bands [80 - 100 nm], [122 - 140 nm],  
148 and [141 - 180 nm] account fairly for 18 % to the production of O(<sup>1</sup>D), while the spectral  
149 range [101 - 120 nm] contribution is 8 %. Regarding the production of O(<sup>1</sup>S), the solar  
150 Lyman  $\alpha$  line accounts for 45 % while the spectral band [90 - 115 nm] is responsible for 40  
151 %. The spectral band between 60 and 90 nm represents roughly 13 % of the production.

## 2.2. Loss reactions

152 While the production reactions are mainly photolysis processes, loss reactions of atomic  
153 oxygen  $O(^1D)$  and  $O(^1S)$  are either collisional processes or radiative decays. Collisional  
154 quenching by water is the predominant loss reaction in the inner coma, while the radiative  
155 processes are very effective far from the nucleus [see e.g. *Bhardwaj and Raghuram, 2012*].  
156 Table 2 summarizes the major loss reactions of the oxygen states  $O(^1D)$  and  $O(^1S)$  taken  
157 into account in the present model when considering water, carbon monoxide, molecular  
158 oxygen and carbon dioxide. The associated rate coefficients are also summarised in Table  
159 2, and computed for a temperature of 50 K. In the case of the volatile densities of 67P  
160 near perihelion, the oxygen state  $O(^1D)$  begins to be efficiently quenched by water for  
161 altitudes below 400 km with a maximal loss rate of about  $1 \text{ s}^{-1}$  at 10 km from the  
162 nucleus as displayed in Figure 4. Regarding the oxygen state  $O(^1S)$ , radiative processes  
163 are effective above 20 km, and the maximum loss rate at 10 km above the nucleus reaches  
164  $2.62 \text{ s}^{-1}$ .

165 Early results of the ROSINA/DFMS instrument have led to the unprecedented detection  
166 of  $N_2$  in comets [*Rubin et al., 2015*]. However, the relative abundance of this molecule  
167 is negligible (with a  $N_2/CO$  ratio of  $(5.70 \pm 0.66) \times 10^{-3}$ ) for efficiently quenching the  
168 produced  $O(^1D)$  and  $O(^1S)$  since the rate coefficients for collisional processes with  $N_2$  are  
169 similar to those with  $CO_2$ , as discussed by *Atkinson et al. [2004]*. Given the presence of  
170  $O_2$ , two additional loss reactions have been considered, listed in Table 2. However, the  
171 impact of  $O_2$  on the total loss rate, which is still dominated by the collisional quenching  
172 by water at low altitudes and by radiative decay otherwise, is negligible.

### 2.3. Red and green line emissions

For evaluating the number densities of O(<sup>1</sup>D) and O(<sup>1</sup>S) within 67P, we solve the continuity equation using a constant radial outflow velocity,  $v$ , of 700 m s<sup>-1</sup>, for steady-state equations and spherical symmetry, such as

$$\frac{1}{r^2} \frac{d}{dr} (r^2 N_i v) = P_i - L_i \quad (3)$$

where  $N_i$  are the number densities for the excited atomic oxygen states, i.e. O(<sup>1</sup>D) and O(<sup>1</sup>S).  $P_i$  and  $L_i$  are the production and loss rates, respectively. The loss term,  $L_i$ , depends on the number densities,  $N_i$ . The equation has to be solved iteratively, starting from  $z = 10$  km. The transport term will not impact the O(<sup>1</sup>S) density because its lifetime is very short (less than 1 s). This is not the case, however, for O(<sup>1</sup>D) with a lifetime of about 130 s, which represents a distance of 90 km for the considered velocity. The computed densities are displayed in Figure 5, along with the radial densities of water, carbon monoxide, carbon dioxide, and molecular oxygen used in our model. For the sake of comparison, the number density of O(<sup>1</sup>D) without transport is also represented.

The difference arising from the inclusion of transport is significant for altitudes lower than 400 km, with a maximum difference for the number density of O(<sup>1</sup>D) of 50% at 90-100 km. In the following, transport will therefore always be taken into account, unless specifically stated otherwise. The attenuation of the solar UV flux is not really pronounced, leading to a constant radial profile for O(<sup>1</sup>D) with a number density of about  $2 \times 10^3$  cm<sup>-3</sup> for altitudes below 100 km. The number density of O(<sup>1</sup>S) peaks at 10 km from the nucleus with a value close to 90 cm<sup>-3</sup>.

192 Emission rate profiles for the red-doublet and green line can be deduced by multiplying  
193 the number densities with the Einstein transition probabilities indicated in Table 2 for  
194 reactions 4, 5, and 10. The green and red-doublet lines are forbidden transition and are  
195 therefore optically thin, making their attenuation by the cometary atmosphere negligible.  
196 The integrated emission intensity along a projected line-of-sight at various cometocentric  
197 distances,  $z$ , is an interesting parameter to be computed from our model for comparison  
198 to remote sensing observations. Considering the maximum extent of the coma to be less  
199 than  $10^4$  km, the computed emissions are estimated at 673 Rayleigh (R) and 493 R for  
200  $O(^1D)$  and  $O(^1S)$ , respectively, for  $z = 10$  km. One Rayleigh (1 R) is defined as a column  
201 emission rate of  $10^6$  photons.cm<sup>-2</sup>.s<sup>-1</sup>. The computed emission intensities decrease at  
202 greater cometocentric distances: 508 R and 72 R for  $O(^1D)$  and  $O(^1S)$ , respectively, for  $z$   
203 = 100 km. We can also consider the green to red-doublet emission intensity ratio (G/R) as  
204 a function of the cometocentric distance. The G/R ratio is generally used for determining  
205 the CO<sub>2</sub> abundances in cometary atmospheres [Decock *et al.*, 2015]. We explore here the  
206 effect of transport on the G/R ratio, as displayed in Figure 6, considering an integration  
207 along the line of sight. With the number densities obtained in this work for 67P, the G/R  
208 ratio peaks at 10 km with a value of 0.73 with transport, and 0.59 without. By considering  
209 the transport, the G/R ratio increases along the line of sight below 400 km. The effect of  
210 transport will be important when the loss rate is dominated by collisional quenching. The  
211 gradient of the loss rate is large for altitudes lower than 400 km for  $O(^1D)$  (see Figure 4).  
212 At higher cometocentric distances, both ratios with and without transport are equivalent  
213 since the major loss reaction is the radiative decay process.

### 3. Discussion

Several parameters affect the number densities of  $O(^1D)$  and  $O(^1S)$ , and therefore the G/R ratio. First, the distance to the Sun impacts directly the water production rate,  $Q$ , as well as the outgassing speed,  $v$ . These modifications affect the absorption of the solar UV flux at each altitude  $z$ , and therefore the reaction rate coefficients. The impact of transport depends on the outgassing speed. As discussed by *Bhardwaj and Raghuram* [2012], the production of  $O(^1S)$  through the photodissociation of  $H_2O$  depends on the chosen yield at the solar Lyman  $\alpha$  line (set to be 0.5 % in our model). The relative abundances of different elements also affect the G/R ratio. In the following, we still consider a distance to the sun of 1.35 AU and we look for the impact of abundance variations for  $CO_2$  and  $O_2$ . We also look for the choice of the partial cross sections for  $CO_2$  and its implication on the G/R ratio. Finally, the G/R ratio will be characterized in a planetary space weather context by looking at the impact of solar activity on the photoproduction rates.

#### 3.1. Impact of cometary $O_2$

We first compare the computed G/R ratio obtained using the complete atmosphere of 67P including molecular oxygen from the previous sections to a molecular-oxygen-free atmosphere as displayed in Figure 7. While the G/R ratio peaks at 10 km with a value of 0.80 without  $O_2$ , it decreases down to 0.73 with  $O_2$ . Its presence thus induces a small difference in the G/R ratio profile. In order to assess whether this difference is significant, we consider a third atmospheric composition without oxygen, with the same CO abundance relative to water of 25 % and a 6.3 %  $CO_2$  abundance relative to water. The computed G/R ratio profile is displayed in green in Figure 7. This 2 % difference of  $CO_2$  gives a similar profile as the one obtained with 8 % of  $CO_2$  and 4 % of  $O_2$ . In the

235 case of 67P with its atmospheric properties, not taking the presence of O<sub>2</sub> into account  
236 leads to an absolute underestimation of the CO<sub>2</sub> abundance relative to water of about  
237 2 %, which represents in fact a relative difference of 25 %.

238 More generally, the increase of CO<sub>2</sub> alone leads to an enhancement of the G/R value,  
239 while it is the opposite for O<sub>2</sub> when using the reaction rate coefficients from Tab. 1.  
240 This is illustrated in Figure 8, where the G/R ratio is given for different configurations  
241 regarding the CO<sub>2</sub> (from 0 % to 20 %) and O<sub>2</sub> (0 %, 4 %, and 8 %) abundances relative  
242 to water. For an amount of 16 % of CO<sub>2</sub> at a distance of 10 km from the nucleus, the  
243 G/R ratio is about 1.02 with 0 % of O<sub>2</sub>. It decreases down to 0.94 for 4 % of O<sub>2</sub> and  
244 down to 0.87 for 8 % of O<sub>2</sub>. At higher projected cometocentric distances, the presence  
245 of O<sub>2</sub> induces a smaller spread for the G/R ratio. At 50 km, the G/R ratio is of about  
246 0.33, 0.30, and 0.28, still with 16 % of CO<sub>2</sub> for an O<sub>2</sub> abundance of 0 %, 4 %, and 8 %,   
247 respectively.

### 3.2. Impact of CO<sub>2</sub> cross sections uncertainties

248 We consider from now on a complete 67P atmospheric composition including H<sub>2</sub>O, CO<sub>2</sub>  
249 (8.3 %), CO (25 %), and O<sub>2</sub> (4 %). The values found in the literature for the reaction rates  
250 of the production of oxygen states O(<sup>1</sup>D) and O(<sup>1</sup>S) from photodissociation of CO<sub>2</sub> are  
251 actually quite diverse and, consequently, so is their ratio. This ratio is > 1 in some studies  
252 [*Raghuram and Bhardwaj*, 2013], and < 1 in others [*Bhardwaj and Raghuram*, 2012]. This  
253 difference comes from the chosen yield used for deducing the partial cross sections leading  
254 to the production of O(<sup>1</sup>D) and O(<sup>1</sup>S) from the total photoabsorption cross section of  
255 CO<sub>2</sub>. To explore its impact on the G/R ratio, we consider here two extreme values, using  
256 two different cross section sets for the photochemistry of carbon dioxide in our model.



257 The first is the one used in the previous section. As a second cross section data set,  
258 we consider the recommended values from the ATMOCIAD database. The  $O(^1S)/O(^1D)$   
259 ratio goes from 0.53 using the values provided in Table 1 to 6.98 using the cross sections  
260 from the ATMOCIAD database. The latter ratio is computed using photo-reactions rates  
261 of  $3.97 \times 10^{-7} \text{s}^{-1}$  and  $5.68 \times 10^{-8} \text{s}^{-1}$  for  $O(^1S)$  and  $O(^1D)$ , respectively, for a distance of  
262 1.35 AU. Using such parameters, the computed emissions are estimated at 639 R and  
263 571 R for  $O(^1D)$  and  $O(^1S)$ , respectively, for  $z = 10$  km. At this distance, the G/R ratio  
264 increases up to 0.89, compared to 0.73. Figure 9 displays the projected G/R ratio from 10  
265 km to  $10^4$  km, using both cross section data sets for a solar UV flux corresponding to an  
266 F10.7 index of 104 (black lines). The lack of knowledge regarding the  $\text{CO}_2$  cross sections  
267 thus leads to an important uncertainty on the computed G/R ratio and emphasizes the  
268 need for accurate  $\text{CO}_2$  cross sections measurements.

### 3.3. Space Weather context

269 Planetary space weather research has started with the exploration of planetary envi-  
270 ronments other than the Earth [Lilensten *et al.*, 2014]. It is today a growing research  
271 area of interest in the framework of future solar system missions such as JUICE [Grasset  
272 *et al.*, 2013] or BepiColombo [Benkhoff *et al.*, 2010]. In this context, we are looking at the  
273 impact of the solar UV flux variability, including the 11-year cycle and solar flares, on the  
274 G/R ratio. To do so, we consider here two additional solar UV values. The first one is a  
275 composite spectrum for a high but steady solar activity, with a F10.7 solar proxy of 195  
276 (red curve in Figure 2). The second one corresponds to the solar UV radiated during an  
277 X-class solar flare (X17) measured by the TIMED/SEE spectrometer on 28 October 2003  
278 (green curve in Figure 2). The variability compared to quiet solar conditions can reach

279 more than 1000% in the XUV spectral range between 0-20 nm, 100% in the EUV (20-120  
280 nm), and 10-20% in the FUV (120-200 nm).

281 Figure 10 displays the different computed G/R ratios according to the different solar  
282 activity levels. We still consider both cross section data sets regarding the production  
283 of O(<sup>1</sup>D) and O(<sup>1</sup>S) through the photodissociation of CO<sub>2</sub>. The ratio generally increases  
284 for higher solar activity. With the ATMOCIAAD database as inputs, the G/R ratio is  
285 of 1.55 for  $z = 10$  km, while it is 1.08 using the PHIDRATES database for the X-17  
286 solar flare. Observations of the red-doublet and green line emissions during a powerful  
287 solar flare could eventually help to constrain the reaction rates of the photodissociation  
288 of CO<sub>2</sub>. Unfortunately, the solar flare must be "comet-effective", which is a rare event.  
289 Considering a less powerful X-1 solar flare from the 15 January 2005, the G/R ratio is  
290 still significantly impacted with values ranging from 1.21 to 0.091 using ATMOCIAAD  
291 and PHIDRATES, respectively. The difference between G/R ratios using ATMOCIAAD  
292 and PHIDRATES databases seems to increase when considering more powerful solar flare  
293 events. These results highlight the fact that more efforts are needed to better constrain  
294 the photodissociation cross sections of CO<sub>2</sub> leading to the production of O(<sup>1</sup>D) and O(<sup>1</sup>S),  
295 and solar flares could be a possible way for doing so.

296 There is also a noticeable impact of the 11-year cycle on the G/R ratio. The variability  
297 induced by such modulation is typically within 50-100% for the EUV, while it is less than  
298 10 % for the FUV. Between medium and high solar activity, the ratio increases from  
299 0.73 to 0.86 (using PHIDRATES) and from 0.89 to 1.11 (using ATMOCIAAD). However,  
300 this impact is actually hidden by the lack of knowledge on the cross sections. The solar  
301 irradiance is also impacted by a 27-day solar modulation from its rotation. However, the

302 induced variability on the solar UV flux is not important enough to have a significant  
303 impact on the G/R ratio. Interestingly, this would mean that knowledge about the solar  
304 UV flux on a rotational time scale is not mandatory when considering the G/R ratio. It  
305 is, however, not the case for the number densities of O(<sup>1</sup>D) and O(<sup>1</sup>S), which are directly  
306 linked to the absolute solar UV values.

#### 4. Conclusions

307 We have presented in this paper a photochemistry-emission coupled model for the  
308 oxygen red-doublet and green lines for comet 67P/Churyumov-Gerasimenko. Using the  
309 ROSINA/DFMS data, an atmospheric composition based on water, CO<sub>2</sub>, CO, and O<sub>2</sub> has  
310 been used. The latter species has never been taken into consideration in such modeling  
311 before. As outputs, we computed the G/R ratio along projected cometocentric distances;  
312 this G/R ratio has often been used for assessing the relative abundance of CO<sub>2</sub>. However,  
313 the impact of O<sub>2</sub> is strong enough to require a revision of such conclusions. The important  
314 results from our present study can be summarised as follows:

- 315 • Not taking the transport of the produced O(<sup>1</sup>D) into account can lead to a significant  
316 underestimation of the G/R ratio for altitudes lower than 400 km, where most of the  
317 emission comes from. The transport can therefore not be neglected in such modeling.
- 318 • CO<sub>2</sub> and O<sub>2</sub> have opposite effects on the G/R ratio. Not taking the presence of  
319 O<sub>2</sub> in cometary atmospheres into account would lead to an underestimation of its CO<sub>2</sub>  
320 abundance. The G/R ratio can therefore not be directly used for assessing the relative  
321 abundance of CO<sub>2</sub> within cometary atmospheres, without knowledge of the O<sub>2</sub> abundance.

322 • CO<sub>2</sub> cross section uncertainties are high, and this requires more studies to better  
323 constrain the O(<sup>1</sup>D) and O(<sup>1</sup>S) production from the photodissociation of CO<sub>2</sub>.

324 • Within a space weather context, we have explored the effect of several solar condi-  
325 tions: a powerful flare has a significant impact on the G/R ratio, and can even be used as  
326 tool for constraining the CO<sub>2</sub> cross sections, assuming that the abundance of O<sub>2</sub> within  
327 the coma is known. Solar activity levels have to be characterized while measuring the  
328 G/R ratio.

329 The ROSINA/DFMS discovery of O<sub>2</sub> at a significant percentage might have been a  
330 surprise at first. The fact that O<sub>2</sub> had never been detected in a comet before seemed a  
331 major objection. In-situ measurements at 1P/Halley with Giotto did not have sufficient  
332 mass resolution to really distinguish <sup>16</sup>O<sub>2</sub> from <sup>32</sup>S and methanol (CH<sub>3</sub>OH) [*Geiss et al.*,  
333 1991], so its possible presence was simply overlooked. In remote sensing observations, no  
334 one has thought of including O<sub>2</sub> in emission models, so that these emissions were ascribed  
335 to CO<sub>2</sub>, even when CO<sub>2</sub> itself was believed to be below the detection level [in the case of  
336 comet C/1996 B2 Hyakutake as modeled by *Bhardwaj and Raghuram*, 2012]. Our findings  
337 that O<sub>2</sub> and CO<sub>2</sub> are in a sense interchangeable as far as the green and red line emissions  
338 are concerned are essential for understanding why measurements of the G/R ratio alone  
339 are insufficient to determine the presence or absence of either CO<sub>2</sub> or O<sub>2</sub> - both are  
340 probably present but in an unknown proportion. Earlier assessments of CO<sub>2</sub> abundances  
341 in cometary atmospheres using the G/R ratio have to be revised in the light of the  
342 unambiguous O<sub>2</sub> detection by ROSINA/DFMS. This will be addressed in a forthcoming  
343 paper considering moderately and highly active comets using a 2D photochemistry model  
344 for different CO<sub>2</sub> and O<sub>2</sub> abundances.

**Acknowledgments.**

Work at BIRA-IASB was supported by the Fonds de la Recherche Scientifique grant PDR T.1073.14 Comparative study of atmospheric erosion, by the Belgian Science Policy Office via PRODEX/ROSINA PEA4000107705 and an Additional Researchers Grant (Ministerial Decree of 2014-12-19), and by the Interuniversity Attraction Pole P7/15 "Planets: tracing the Transfer, Origin, Preservation and Evolution of their Reservoirs".

Work at the ULB was supported by the Belgian Fund for Scientific Research - FNRS.

Work at UoB was funded by the State of Bern, the Swiss National Science Foundation, and by the European Space Agency PRODEX Program. Work at Southwest Research institute was supported by subcontract no. 1496541 from the Jet Propulsion Laboratory. Work at the University of Michigan was funded by NASA under contract JPL-1266313. GG was supported by NASA Astrobiology Institute Grant NNX15AE05G and by the NASA HIDEE program. Rosetta is an ESA mission with contributions from its member states and NASA. The results from Rosetta and ROSINA would not be possible without the work of the many engineers, technicians, and scientists involved in the mission over the past 20 years, whose contributions are gratefully acknowledged. All Rosetta/ROSINA data are available on request until they are released to the PSA archive of ESA ([www.rssd.esa.int/PSA](http://www.rssd.esa.int/PSA)) and to the PDS archive of NASA. The solar UV flux data were obtained from the LISIRD database (<http://lasp.colorado.edu/lisird/ssi/>). The cross sections data used in this paper can be obtained from the PHIDRATES database (<http://phidrates.space.swri.edu/>), and from the ATMOCIAAD database which is available from the authors upon request ([Guillaume.P.Gronoff@nasa.gov](mailto:Guillaume.P.Gronoff@nasa.gov)). The authors would

367 like to thank the anonymous reviewers for their insightful comments and suggestions that  
368 have contributed to improve this paper.

## References

- 369 Altwegg, K., H. Balsiger, A. Bar-Nun, J. J. Berthelier, A. Bieler, P. Bochsler, C. Briois,  
370 U. Calmonte, M. Combi, J. De Keyser, P. Eberhardt, B. Fiethe, S. Fuselier, S. Gasc,  
371 T. I. Gombosi, K. C. Hansen, M. Hässig, A. Jäckel, E. Kopp, A. Korth, L. LeRoy,  
372 U. Mall, B. Marty, O. Mousis, E. Neefs, T. Owen, H. Rème, M. Rubin, T. Sémon, C.-  
373 Y. Tzou, H. Waite, and P. Wurz (2015), 67P/Churyumov-Gerasimenko, a Jupiter family  
374 comet with a high D/H ratio, *Science*, *347*(27), 1261952, doi:10.1126/science.1261952.
- 375 Atkinson, R., D. L. Baulch, R. A. Cox, J. N. Crowley, R. F. Hampson, R. G. Hynes, M. E.  
376 Jenkin, M. J. Rossi, and J. Troe (2004), Evaluated kinetic and photochemical data for  
377 atmospheric chemistry: Volume i - gas phase reactions of  $\text{o}_x$ ,  $\text{ho}_x$ ,  $\text{no}_x$  and  $\text{so}_x$  species,  
378 *Atmospheric Chemistry and Physics*, *4*(6), 1461–1738, doi:10.5194/acp-4-1461-2004.
- 379 Balsiger, H., K. Altwegg, P. Bochsler, P. Eberhardt, J. Fischer, S. Graf, A. Jäckel,  
380 E. Kopp, U. Langer, M. Mildner, J. Müller, T. Riesen, M. Rubin, S. Scherer, P. Wurz,  
381 S. Wüthrich, E. Arijs, S. Delanoye, J. de Keyser, E. Neefs, D. Nevejans, H. Rème,  
382 C. Aoustin, C. Mazelle, J.-L. Médale, J. A. Sauvaud, J.-J. Berthelier, J.-L. Bertaux,  
383 L. Duvet, J.-M. Illiano, S. A. Fuselier, A. G. Ghielmetti, T. Magoncelli, E. G. Shelley,  
384 A. Korth, K. Heerlein, H. Lauche, S. Livi, A. Loose, U. Mall, B. Wilken, F. Gliem,  
385 B. Fiethe, T. I. Gombosi, B. Block, G. R. Carignan, L. A. Fisk, J. H. Waite, D. T.  
386 Young, and H. Wollnik (2007), Rosina Rosetta Orbiter Spectrometer for Ion and Neu-  
387 tral Analysis, *Space Science Reviews*, *128*, 745–801, doi:10.1007/s11214-006-8335-3.

- 388 Benkhoff, J., J. van Casteren, H. Hayakawa, M. Fujimoto, H. Laakso, M. Novara, P. Ferri,  
389 H. R. Middleton, and R. Ziethe (2010), BepiColombo—Comprehensive exploration of  
390 Mercury: Mission overview and science goals, *Planetary and Space Science*, 58, 2–20,  
391 doi:10.1016/j.pss.2009.09.020.
- 392 Bhardwaj, A., and S. Raghuram (2012), A Coupled Chemistry-emission Model for Atomic  
393 Oxygen Green and Red-doublet Emissions in the Comet C/1996 B2 Hyakutake, *Astro-*  
394 *physical Journal*, 748, 13, doi:10.1088/0004-637X/748/1/13.
- 395 Bieler, A., K. Altwegg, H. Balsiger, A. Bar-Nun, J. J. Berthelier, P. Bochsler, C. Briois,  
396 U. Calmonte, M. Combi, J. De Keyser, E. F. van Dishoeck, B. Fiethe, S. Fuselier,  
397 S. Gasc, T. I. Gombosi, K. C. Hansen, M. Hässig, A. Jäckel, E. Kopp, A. Korth,  
398 L. LeRoy, U. Mall, R. Maggiolo, B. Marty, O. Mousis, H. Rème, M. Rubin, T. Sémon,  
399 C.-Y. Tzou, H. Waite, C. Walsh, and P. Wurz (2015), Abundant molecular oxygen in  
400 the coma of 67P/Churyumov-Gerasimenko, *Nature*, *in press*.
- 401 Cochran, A. L. (2008), Atomic oxygen in the comae of comets, *Icarus*, 198, 181–188,  
402 doi:10.1016/j.icarus.2008.06.007.
- 403 Decock, A., E. Jehin, D. Hutsemékers, and J. Manfroid (2013), Forbidden oxygen lines in  
404 comets at various heliocentric distances, *Astron. Astrophys*, 555, A34, doi:10.1051/0004-  
405 6361/201220414.
- 406 Decock, A., E. Jehin, P. Rousselot, D. Hutsemékers, J. Manfroid, S. Raghuram, A. Bhard-  
407 waj, and B. Hubert (2015), Forbidden oxygen lines at various nucleocentric distances  
408 in comets, *Astron. Astrophys*, 573, A1, doi:10.1051/0004-6361/201424403.
- 409 Evans, J. S., M. H. Stevens, J. D. Lumpe, N. M. Schneider, A. I. F. Stewart, J. Deighan,  
410 S. K. Jain, M. S. Chaffin, M. Crismani, A. Stiepen, W. E. McClintock, G. M. Holsclaw,

- 411 F. Lefvre, D. Y. Lo, J. T. Clarke, F. G. Eparvier, E. M. B. Thiemann, P. C. Chamberlin,  
412 S. W. Bougher, J. M. Bell, and B. M. Jakosky (2015), Retrieval of co<sub>2</sub> and n<sub>2</sub> in  
413 the martian thermosphere using dayglow observations by iuvs on maven, *Geophysical*  
414 *Research Letters*, pp. n/a–n/a, doi:10.1002/2015GL065489.
- 415 Fischer, C. F., and G. Tachiev (2004), Breitpauli energy levels, lifetimes, and transition  
416 probabilities for the beryllium-like to neon-like sequences, *Atomic Data and Nuclear*  
417 *Data Tables*, 87(1), 1 – 184, doi:http://dx.doi.org/10.1016/j.adt.2004.02.001.
- 418 Geiss, J., K. Altwegg, E. Anders, H. Balsiger, A. Meier, E. G. Shelley, W.-H. Ip, H. Rosen-  
419 bauer, and M. Neugebauer (1991), Interpretation of the ion mass spectra in the mass  
420 per charge range 25-35 amu/e obtained in the inner coma of Halley's comet by the  
421 HIS-sensor of the Giotto IMS experiment, *Astron. Astrophys*, 247, 226–234.
- 422 Grasset, O., M. K. Dougherty, A. Coustenis, E. J. Bunce, C. Erd, D. Titov, M. Blanc,  
423 A. Coates, P. Drossart, L. N. Fletcher, H. Hussmann, R. Jaumann, N. Krupp, J.-P. Le-  
424 breton, O. Prieto-Ballesteros, P. Tortora, F. Tosi, and T. Van Hoolst (2013), JUpiter ICy  
425 moons Explorer (JUICE): An ESA mission to orbit Ganymede and to characterise the  
426 Jupiter system, *Planetary and Space Science*, 78, 1–21, doi:10.1016/j.pss.2012.12.002.
- 427 Gronoff, G., C. S. Wedlund, C. J. Mertens, J. Liliensten, R. Lillis, and P. V. Johnson  
428 (2011), The AtMoCIAD database, in *EPSC-DPS Joint Meeting 2011*, p. 1259.
- 429 Gronoff, G., C. Simon Wedlund, C. J. Mertens, and R. J. Lillis (2012a), Computing  
430 uncertainties in ionosphere-airglow models: I. Electron flux and species production  
431 uncertainties for Mars, *Journal of Geophysical Research (Space Physics)*, 117, A04306,  
432 doi:10.1029/2011JA016930.



- 433 Gronoff, G., C. Simon Wedlund, C. J. Mertens, M. Barthélemy, R. J. Lillis, and  
434 O. Witasse (2012b), Computing uncertainties in ionosphere-airglow models: II. The  
435 Martian airglow, *Journal of Geophysical Research (Space Physics)*, *117*, A05309, doi:  
436 10.1029/2011JA017308.
- 437 Gronoff, G., A. Rahmati, C. S. Wedlund, C. J. Mertens, T. E. Cravens, and E. Kallio  
438 (2014), The precipitation of keV energetic oxygen ions at Mars and their effects dur-  
439 ing the comet Siding Spring approach, *Geophys. Res. Lett.*, , *41*, 4844–4850, doi:  
440 10.1002/2014GL060902.
- 441 Haser, L. (1957), Distribution d'intensité dans la tête d'une comète, *Bulletin de la Societe*  
442 *Royale des Sciences de Liege*, *43*, 740–750.
- 443 Hässig, M., K. Altwegg, H. Balsiger, A. Bar-Nun, J. J. Berthelier, A. Bieler, P. Bochsler,  
444 C. Briois, U. Calmonte, M. Combi, J. De Keyser, P. Eberhardt, B. Fiethe, S. A. Fuselier,  
445 M. Galand, S. Gasc, T. I. Gombosi, K. C. Hansen, A. Jäckel, H. U. Keller, E. Kopp,  
446 A. Korth, E. Kührt, L. Le Roy, U. Mall, B. Marty, O. Mousis, E. Neefs, T. Owen,  
447 H. Rème, M. Rubin, T. Sémon, C. Tornow, C.-Y. Tzou, J. H. Waite, and P. Wurz (2015),  
448 Time variability and heterogeneity in the coma of 67P/Churyumov-Gerasimenko, *Sci-*  
449 *ence*, *347*(1), aaa0276, doi:10.1126/science.aaa0276.
- 450 Huebner, W., and J. Mukherjee (2015), Photoionization and photodissociation rates in  
451 solar and blackbody radiation fields, *Planetary and Space Science*, *106*, 11 – 45, doi:  
452 <http://dx.doi.org/10.1016/j.pss.2014.11.022>.
- 453 Huestis, D. L., T. G. Slangier, B. D. Sharpee, and J. L. Fox (2010), Chemical origins of  
454 the Mars ultraviolet dayglow, *Faraday Discussions*, *147*, 307, doi:10.1039/c003456h.

- 455 Le Roy, L., Altwegg, K., Balsiger, H., Berthelier, J.-J., Bieler, A., Briois, C., Calmonte, U.,  
456 Combi, M. R., De Keyser, J., Dhooghe, F., Fiethe, B., Fuselier, S. A., Gasc, S., Gombosi,  
457 T. I., Hssig, M., Jckel, A., Rubin, M., and Tzou, C.-Y. (2015), The inventory of the  
458 volatiles on comet 67p/churyumov-gerasimenko from rosetta/rosina, *Astron. Astrophys*,  
459 doi:10.1051/0004-6361/201526450.
- 460 Lee, L. C., T. G. Slanger, G. Black, and R. L. Sharpless (1977), Quantum yields for the  
461 production of O(<sup>1</sup>D) from photodissociation of O<sub>2</sub> at 1160-1770 Å, *J. Chem. Phys.*, *67*,  
462 5602–5606.
- 463 Lilensten, J., A. J. Coates, V. Dehant, T. Dudok de Wit, R. B. Horne, F. Leblanc,  
464 J. Luhmann, E. Woodfield, and M. Barthélemy (2014), What characterizes planetary  
465 space weather?, *Astronomy and Astrophysics Reviews*, *22*, 79, doi:10.1007/s00159-014-  
466 0079-6.
- 467 McClintock, W. E., M. Snow, and T. N. Woods (2005), Solar-Stellar Irradiance Com-  
468 parison Experiment II (SOLSTICE II): Pre-Launch and On-Orbit Calibrations, *Solar*  
469 *Physics*, *230*, 259–294, doi:10.1007/s11207-005-1585-5.
- 470 McKay, A. J., N. J. Chanover, J. P. Morgenthaler, A. L. Cochran, W. M. Harris, and N. D.  
471 Russo (2012), Forbidden oxygen lines in Comets C/2006 W3 Christensen and C/2007  
472 Q3 Siding Spring at large heliocentric distance: Implications for the sublimation of  
473 volatile ices, *Icarus*, *220*, 277–285, doi:10.1016/j.icarus.2012.04.030.
- 474 McKay, A. J., N. J. Chanover, J. P. Morgenthaler, A. L. Cochran, W. M. Harris, and  
475 N. D. Russo (2013), Observations of the forbidden oxygen lines in DIXI target Comet  
476 103P/Hartley, *Icarus*, *222*, 684–690, doi:10.1016/j.icarus.2012.06.020.

- 477 McKay, A. J., A. L. Cochran, M. A. DiSanti, G. Villanueva, N. D. Russo, R. J. V. Jr.,  
478 J. P. Morgenthaler, W. M. Harris, and N. J. Chanover (2015), Evolution of h<sub>2</sub>o, co,  
479 and {CO<sub>2</sub>} production in comet c/2009 {P1} garradd during the 20112012 apparition,  
480 *Icarus*, *250*, 504 – 515, doi:http://dx.doi.org/10.1016/j.icarus.2014.12.023.
- 481 Morgenthaler, J. P., W. M. Harris, and M. R. Combi (2007), Large aperture o i 6300  
482 observations of comet hyakutake: Implications for the photochemistry of oh and o i  
483 production in comet hale-bopp, *The Astrophysical Journal*, *657*(2), 1162.
- 484 Raghuram, S., and A. Bhardwaj (2013), Model for atomic oxygen visible line emissions  
485 in Comet C/1995 O1 Hale-Bopp, *Icarus*, *223*, 91–104, doi:10.1016/j.icarus.2012.11.032.
- 486 Raghuram, S., and A. Bhardwaj (2014), Photochemistry of atomic oxygen green and red-  
487 doublet emissions in comets at larger heliocentric distances, *Astron. Astrophys.*, , *566*,  
488 A134, doi:10.1051/0004-6361/201321921.
- 489 Rottman, G. (2005), The SORCE Mission, *Solar Physics*, *230*, 7–25, doi:10.1007/s11207-  
490 005-8112-6.
- 491 Rubin, M., K. Altwegg, H. Balsiger, A. Bar-Nun, J.-J. Berthelier, A. Bieler, P. Bochsler,  
492 C. Briois, U. Calmonte, M. Combi, J. De Keyser, F. Dhooghe, P. Eberhardt, B. Fi-  
493 ethe, S. A. Fuselier, S. Gasc, T. I. Gombosi, K. C. Hansen, M. Hässig, A. Jäckel,  
494 E. Kopp, A. Korth, L. Le Roy, U. Mall, B. Marty, O. Mousis, T. Owen, H. Rème,  
495 T. Sémon, C.-Y. Tzou, J. H. Waite, and P. Wurz (2015), Molecular nitrogen in comet  
496 67P/Churyumov-Gerasimenko indicates a low formation temperature, *Science*, *348*,  
497 232–235, doi:10.1126/science.aaa6100.
- 498 Slanger, T. G., P. C. Cosby, B. D. Sharpee, K. R. Minschwaner, and D. E. Siskind (2006),  
499 O(<sup>1</sup>S → <sup>1</sup>D, <sup>3</sup>P) branching ratio as measured in the terrestrial nightglow, *Journal of*

- 500 *Geophysical Research (Space Physics)*, 111, A12,318, doi:10.1029/2006JA011972.
- 501 Stuhl, F., and K. H. Welge (1969), Deactivation of o(1s) and o2(b1g+), *Canadian Journal*  
502 *of Chemistry*, 47(10), 1870–1877, doi:10.1139/v69-306.
- 503 Wiese, W. L., J. R. Fuhr, and T. M. Deters (1996), *Atomic transition probabilities of*  
504 *carbon, nitrogen, and oxygen : a critical data compilation*.
- 505 Woods, T. N., F. G. Eparvier, S. M. Bailey, P. C. Chamberlin, J. Lean, G. J. Rottman,  
506 S. C. Solomon, W. K. Tobiska, and D. L. Woodraska (2005), Solar EUV Experi-  
507 ment (SEE): Mission overview and first results, *Journal of Geophysical Research (Space*  
508 *Physics)*, 110, 1312–+, doi:10.1029/2004JA010765.
- 509 Woods, T. N., P. C. Chamberlin, W. K. Peterson, R. R. Meier, P. G. Richards, D. J. Strick-  
510 land, G. Lu, L. Qian, S. C. Solomon, B. A. Iijima, A. J. Mannucci, and B. T. Tsurutani  
511 (2008), XUV Photometer System (XPS): Improved Solar Irradiance Algorithm Using  
512 CHIANTI Spectral Models, *Solar Physics*, 250, 235–267, doi:10.1007/s11207-008-9196-  
513 6.

**Figure 1.** Number densities considered in the model based on the ROSINA/DFMS data and on Haser's formula, for water (in red), CO (in blue), O<sub>2</sub> (in black), and CO<sub>2</sub> (in green) using a water production rate of  $4 \times 10^{27} \text{ s}^{-1}$  and an outgassing speed of  $700 \text{ m s}^{-1}$  at 1.35 AU.

**Figure 2.** Solar UV fluxes for a heliocentric distance of 1.35 AU for July 2015 (black curve), for high solar activity condition with  $F_{10.7} = 195$  (red curve), and for the X17 flare occurring on 28 October 2003 (green curve).

**Table 1.** Major production reactions of O(<sup>1</sup>D) and O(<sup>1</sup>S), and associated reaction rate coefficients (in s<sup>-1</sup>). The photolysis rate coefficients are given at the top of the atmosphere, and the differences between the top of the atmosphere and at 10 km altitude are indicated in parentheses.

Reaction	Rate Coefficients
H <sub>2</sub> O + hν → O( <sup>1</sup> D) + H <sub>2</sub>	4.91×10 <sup>-7</sup> (-3%)
CO <sub>2</sub> + hν → O( <sup>1</sup> D) + CO	5.52×10 <sup>-7</sup> (-7.3%)
CO + hν → O( <sup>1</sup> D) + C	2.28×10 <sup>-8</sup> (-11.8%)
O <sub>2</sub> + hν → O( <sup>1</sup> D) + O	1.46×10 <sup>-6</sup> (-1.21%)
H <sub>2</sub> O + hν → O( <sup>1</sup> S) + H <sub>2</sub>	2.55×10 <sup>-8</sup> (-2.7%)
CO <sub>2</sub> + hν → O( <sup>1</sup> S) + CO	2.93×10 <sup>-7</sup> (-8.24%)
CO + hν → O( <sup>1</sup> S) + C	1.78×10 <sup>-8</sup> (-11.8%)
O <sub>2</sub> + hν → O( <sup>1</sup> S) + O	4.5×10 <sup>-9</sup> (-8.92%)

**Figure 3.** Top panel: calculated radial profiles for the volumetric production of O(<sup>1</sup>D) (in black) from 10 to 10<sup>4</sup> km, along with its contribution from the photodissociation of water (red dashed line), of CO<sub>2</sub> (green), of O<sub>2</sub> (blue dashed line), and of CO (dark blue). The contribution to the O(<sup>1</sup>D) production through radiative decay of O(<sup>1</sup>S) is also displayed (dashed black line). Bottom panel: Same color code for the production of O(<sup>1</sup>S). The radial profiles are calculated with a water production rate of 4×10<sup>27</sup> s<sup>-1</sup> for 25 % CO, 8.3 % CO<sub>2</sub> and 4 % of O<sub>2</sub> abundances relative to water at 1.35 AU.

**Table 2.** Major loss reactions of O(<sup>1</sup>D) and O(<sup>1</sup>S), and associated rate coefficients computed with the composite solar spectrum at 1.35 AU and the different partial cross sections described within the text.

Reaction	Rate Coefficients <sup>a</sup>
(1) O( <sup>1</sup> D) + H <sub>2</sub> O → OH + OH	$k_1=2.2\times 10^{-10}$
(2) O( <sup>1</sup> D) + CO <sub>2</sub> → O + CO <sub>2</sub>	$k_2=6.8\times 10^{-11}e^{-117/T}$
(3) O( <sup>1</sup> D) + CO → O + CO	$k_3=5.5\times 10^{-10}e^{-625/T}$
(4) O( <sup>1</sup> D) → O( <sup>3</sup> P) + $h\nu$ (630 nm)	$A_1 = 6.478\times 10^{-3}$
(5) O( <sup>1</sup> D) → O( <sup>3</sup> P) + $h\nu$ (634.4 nm)	$A_2 = 2.097\times 10^{-3}$
(6) O( <sup>1</sup> D) + O <sub>2</sub> → O( <sup>3</sup> P) + O <sub>2</sub>	$k_{11} = 3.2 \times 10^{-11}$
(7) O( <sup>1</sup> S) + H <sub>2</sub> O → OH + OH	$k_6=3\times 10^{-10}$
(8) O( <sup>1</sup> S) + CO <sub>2</sub> → O + CO <sub>2</sub>	$k_7=3.1\times 10^{-11}e^{-1330/T}$
(9) O( <sup>1</sup> S) + CO → O + CO	$k_8=3.21\times 10^{-12}e^{-1327/T}$
(10) O( <sup>1</sup> S) → O( <sup>1</sup> D) + $h\nu$ (557.7 nm)	$A_3 = 1.26$
(11) O( <sup>1</sup> S) → O( <sup>3</sup> P) + $h\nu$ (297.7 nm)	$A_4 = 0.134$
(12) O( <sup>1</sup> S) + O <sub>2</sub> → O( <sup>3</sup> P) + O <sub>2</sub>	$k_{12} = 3.2\times 10^{-13}$

<sup>a</sup> Units are cm<sup>3</sup>s<sup>-1</sup> for two-body reactions,  $A_i$  are in s<sup>-1</sup>.  $k_i$  are from *Atkinson et al.* [2004]. Einstein transition probabilities are from *Fischer and Tachiev* [2004] ( $A_1$  and  $A_2$ ), *Wiese et al.* [1996] for  $A_3$  and *Slanger et al.* [2006] for  $A_4$ .

**Figure 4.** Total loss rates for O(<sup>1</sup>D) (thick blue) and O(<sup>1</sup>S) (thick red). The partial loss rates due to radiative decay (dotted-dashed lines) and collision quenching by H<sub>2</sub>O (dotted line) are also represented for O(<sup>1</sup>D) (in blue) and O(<sup>1</sup>S) (in red).

**Figure 5.** Number densities considered in the model based on the ROSINA/DFMS data and on Haser's formula, for water (in red), CO (in blue), O<sub>2</sub> (in black), and CO<sub>2</sub> (in green) using a water production rate of  $4 \times 10^{27} \text{ s}^{-1}$  at 1.35 AU. The computed number densities for O(<sup>1</sup>D) with (dashed-dotted red line) and without transport (dashed black line) and for O(<sup>1</sup>S) (dashed-dotted black line) are also displayed.

**Figure 6.** G/R ratio profile for 67P from 10 to 10<sup>4</sup> km for a line-of-sight crossing the projected cometocentric distance with (in red) and without transport (in black). The G/R ratio profile is calculated with a water production rate of  $4 \times 10^{27} \text{ s}^{-1}$  for 25 % CO, 8.3 % CO<sub>2</sub> and 4 % of O<sub>2</sub> abundances relative to water at 1.35 AU.

**Figure 7.** G/R ratio profile for 67P from 10 to 10<sup>4</sup> km for a line-of-sight crossing the projected cometocentric distance for several 67P atmospheric compositions: 8.3 % CO<sub>2</sub> and 0 % O<sub>2</sub> (red line), 8.3 % CO<sub>2</sub> and 4 % O<sub>2</sub> (dashed black line), and 6.3 % CO<sub>2</sub> and 0 % O<sub>2</sub> (green line). The G/R ratio profile is calculated with a water production rate of  $4 \times 10^{27} \text{ s}^{-1}$  at 1.35 AU.

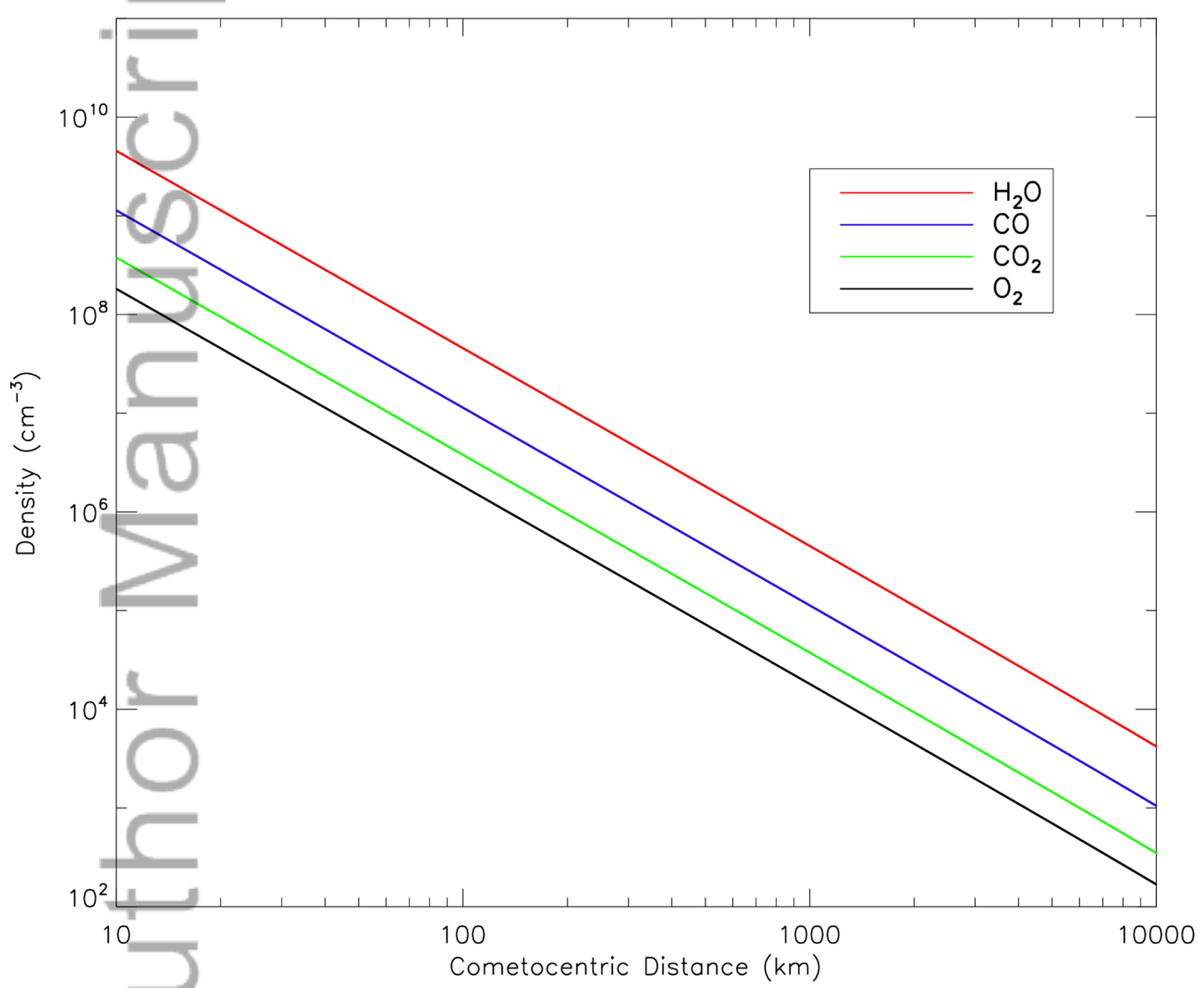
**Figure 8.** Modeled G/R ratio profile for 67P from 10 to 10<sup>3</sup> km for a line-of-sight crossing the projected cometocentric distance for several 67P atmospheric compositions regarding the CO<sub>2</sub> and O<sub>2</sub> abundances relative to water. The color code indicates the G/R ratio, which is calculated with a water production rate of  $4 \times 10^{27} \text{ s}^{-1}$  at 1.35 AU. .



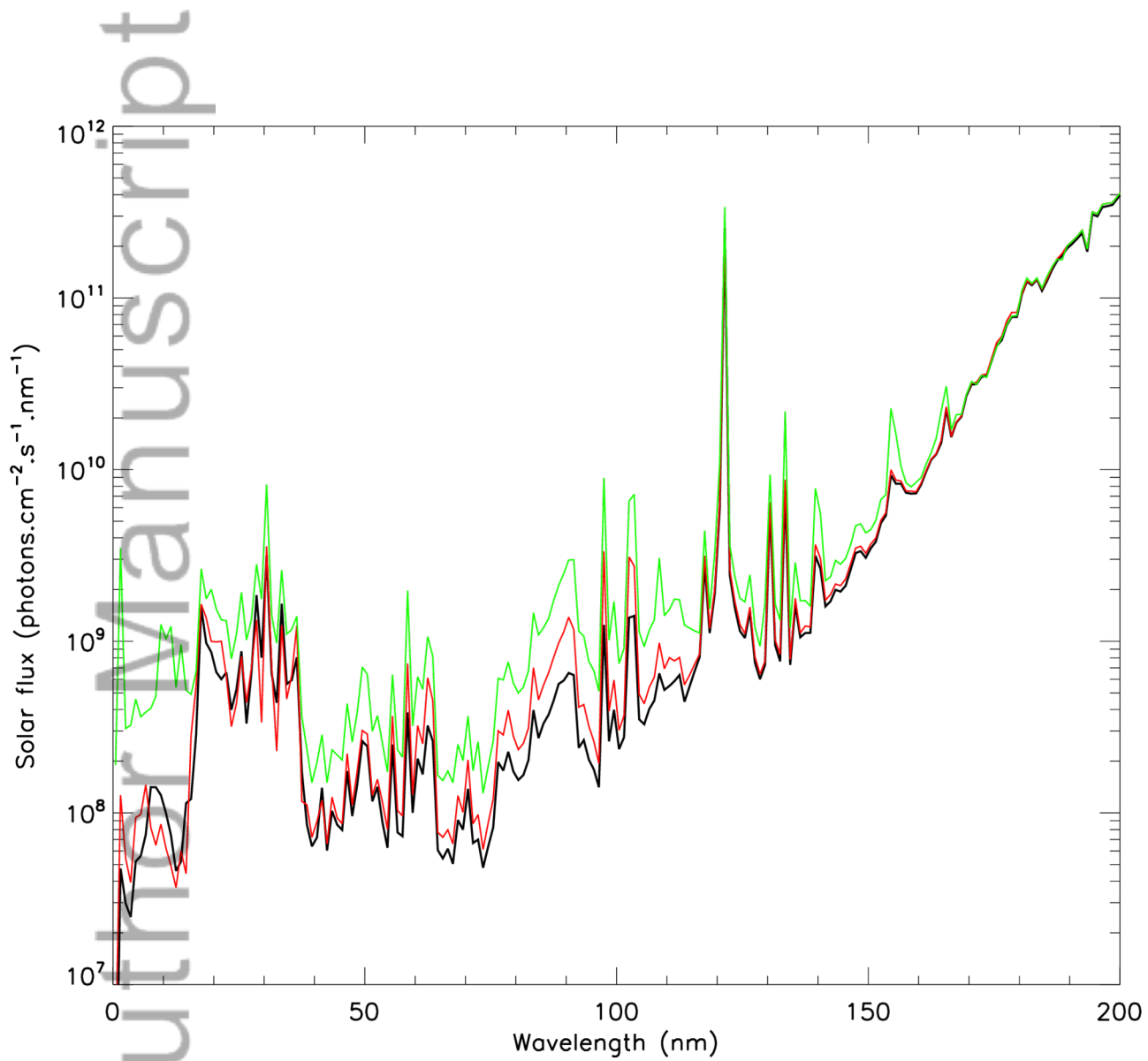
**Figure 9.** G/R ratio profile for 67P from 10 to  $10^4$  km for a line-of-sight crossing the projected cometocentric distance according to different cross section data sets for  $\text{CO}_2$ , using PHIDRATES (in black) and ATMOCIAD (in red). The G/R ratio profile is calculated for with a water production rate of  $4 \times 10^{27} \text{ s}^{-1}$  for 25 % CO, 8.3 %  $\text{CO}_2$  and 4 % of  $\text{O}_2$  abundances relative to water at 1.35 AU.

**Figure 10.** G/R ratio profile for 67P from 10 to  $10^4$  km for a line-of-sight crossing the projected cometocentric distance according to different levels of solar activity: for medium solar conditions with solar F10.7 proxies of 104 (black lines) and 195 (red lines). The green lines correspond to the G/R ratio computed with the X17 solar flare spectrum as input. Dashed lines correspond to the computed G/R ratio using cross sections from PHIDRATES for  $\text{CO}_2$ , while solid lines use the ones from ATMOCIAD. The G/R ratio profile is calculated with a water production rate of  $4 \times 10^{27} \text{ s}^{-1}$  for 25 % CO, 8.3 %  $\text{CO}_2$  and 4 % of  $\text{O}_2$  abundances relative to water at 1.35 AU.

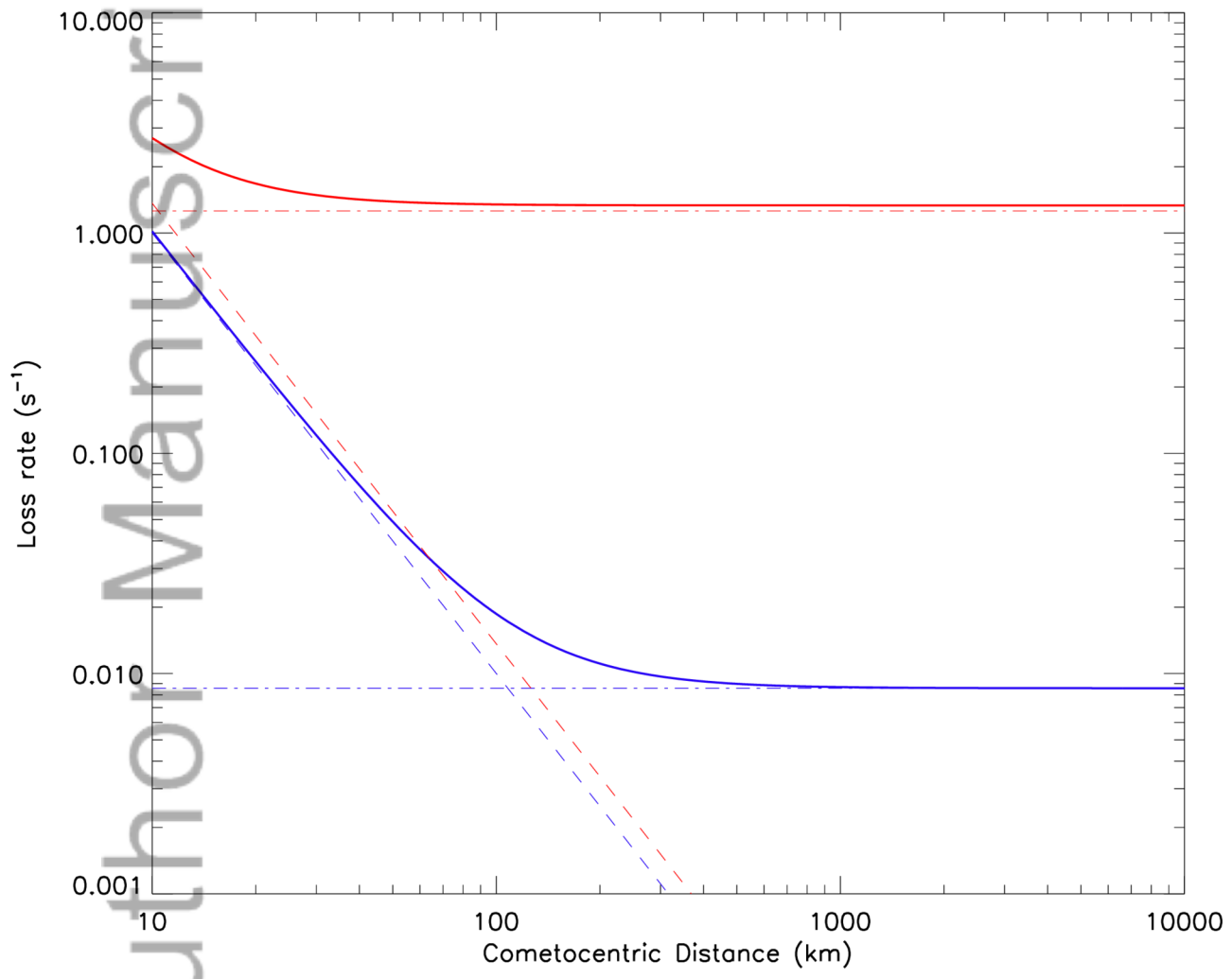
Author Manuscript

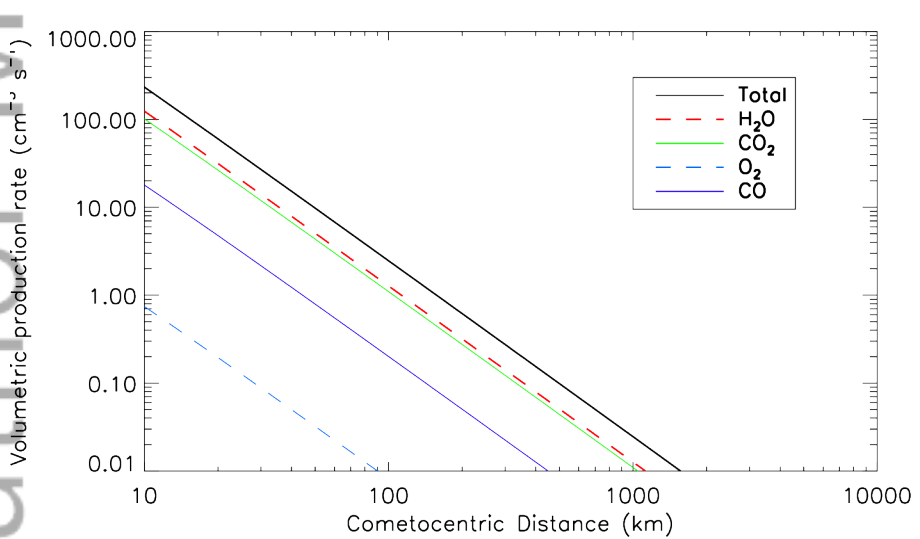
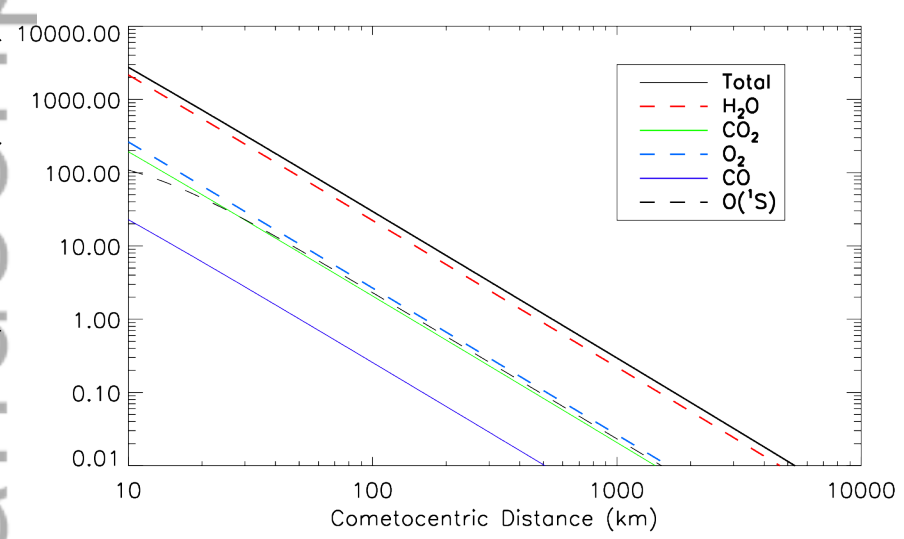


2015ja022013-f00-z-

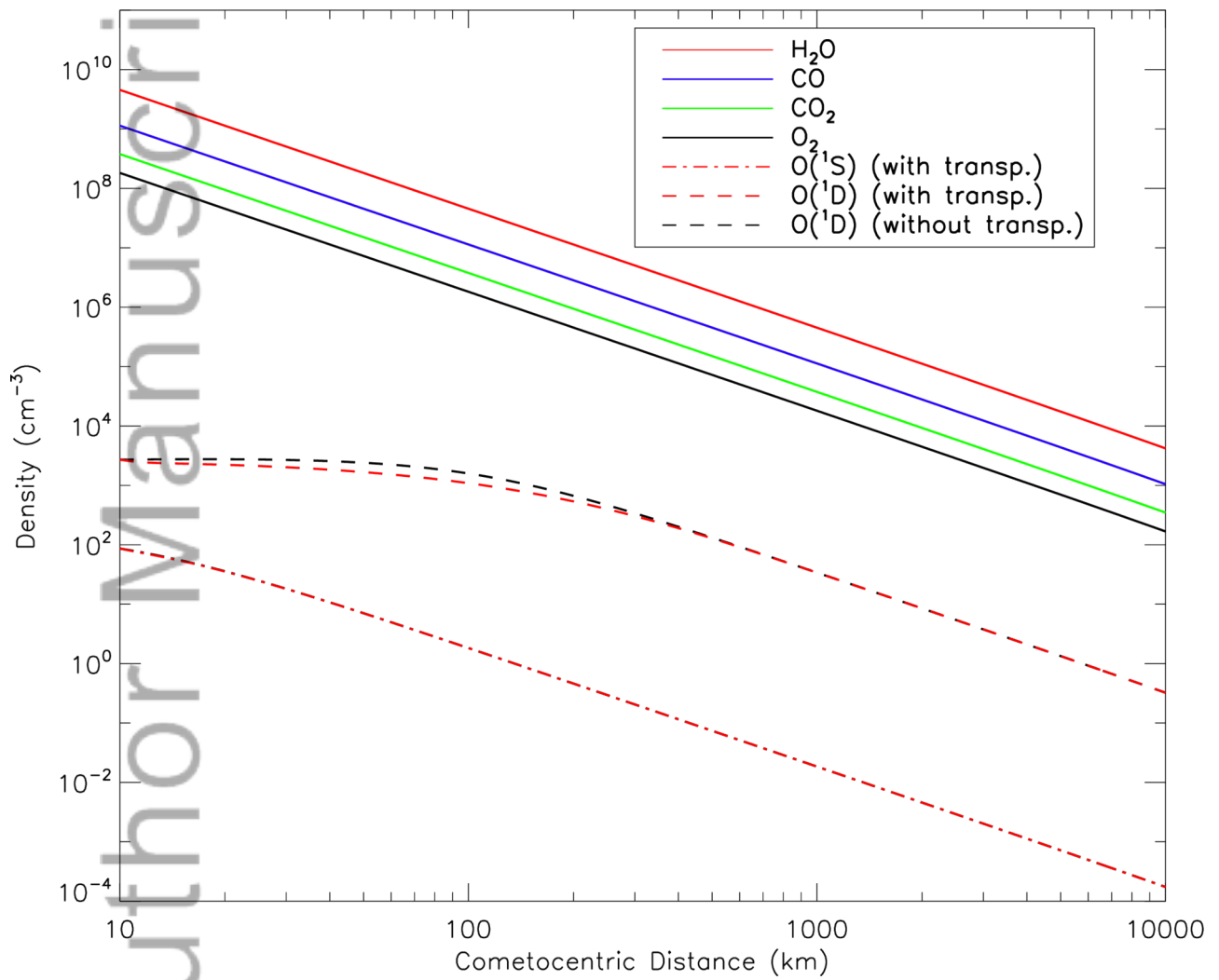


2015ja022013-f01-z-

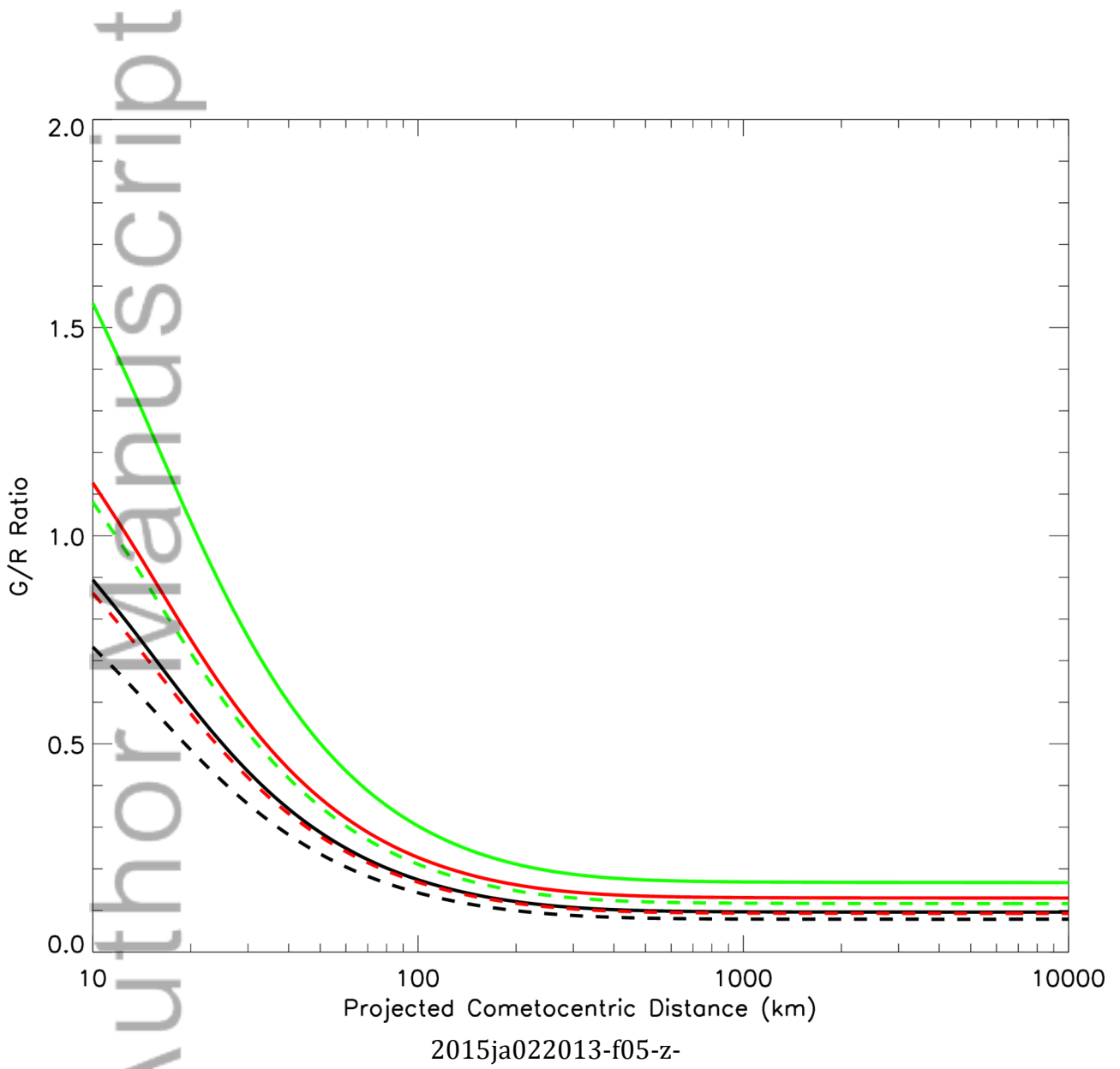


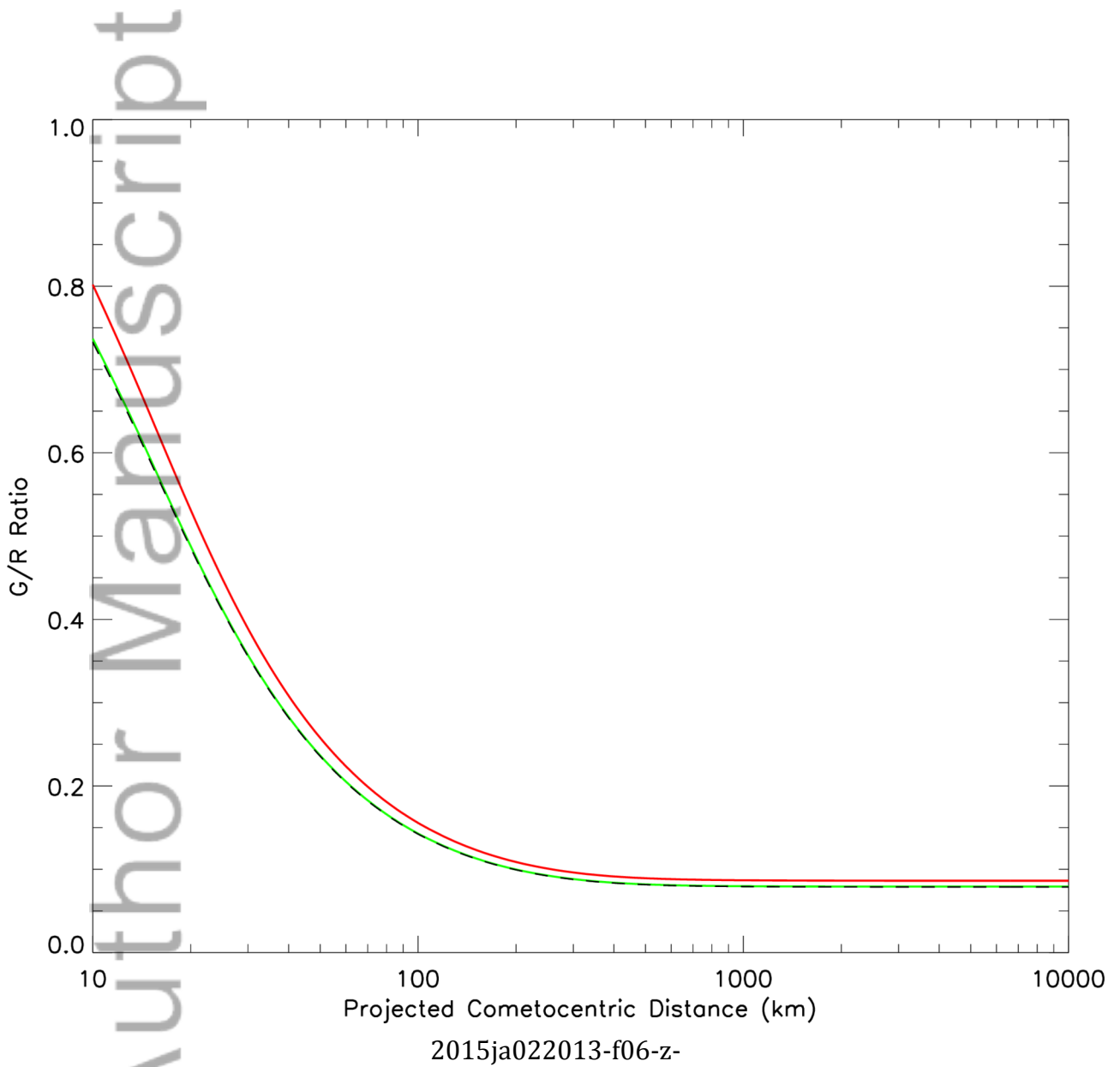


2015ja022013-f03-z-

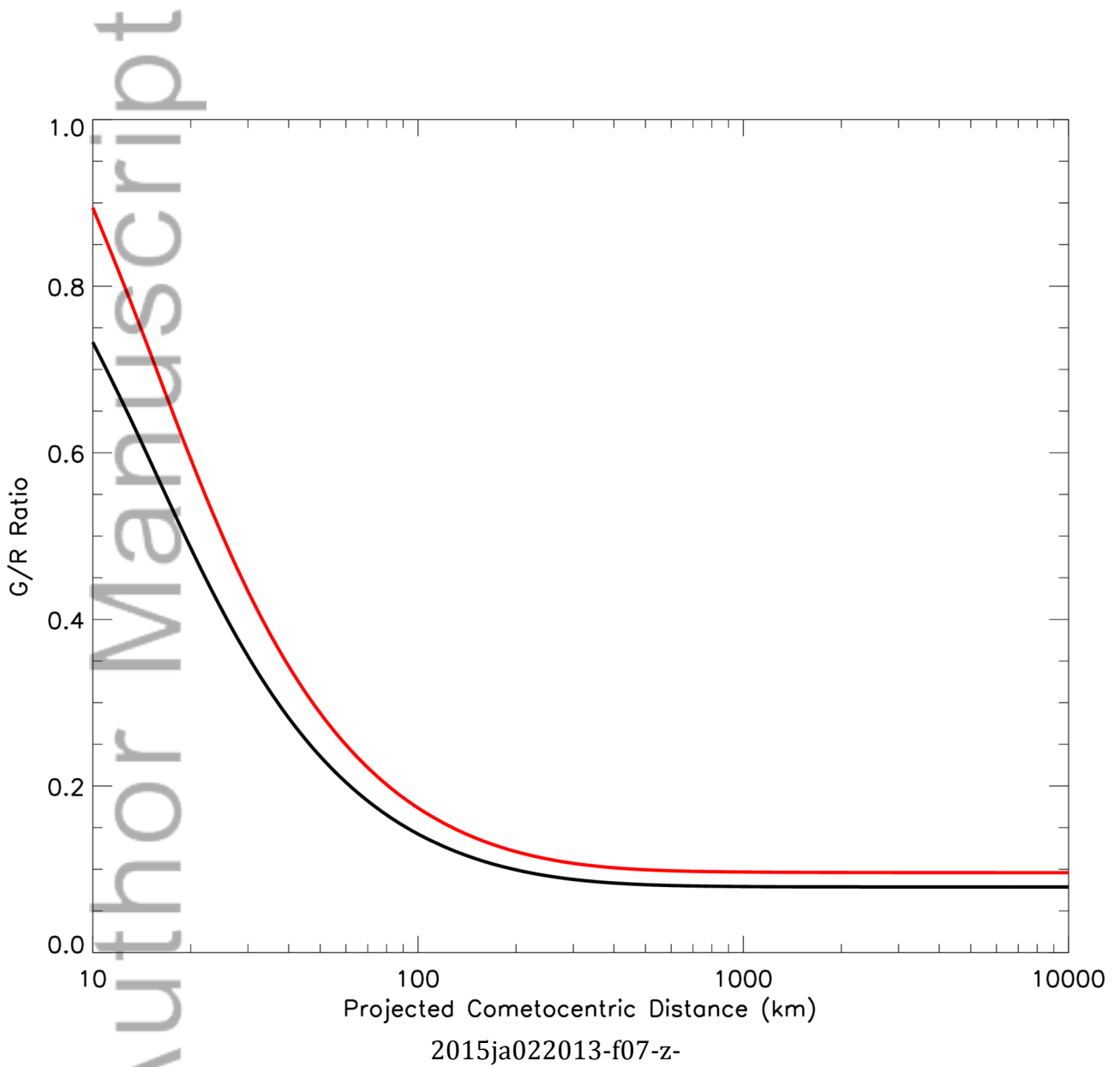


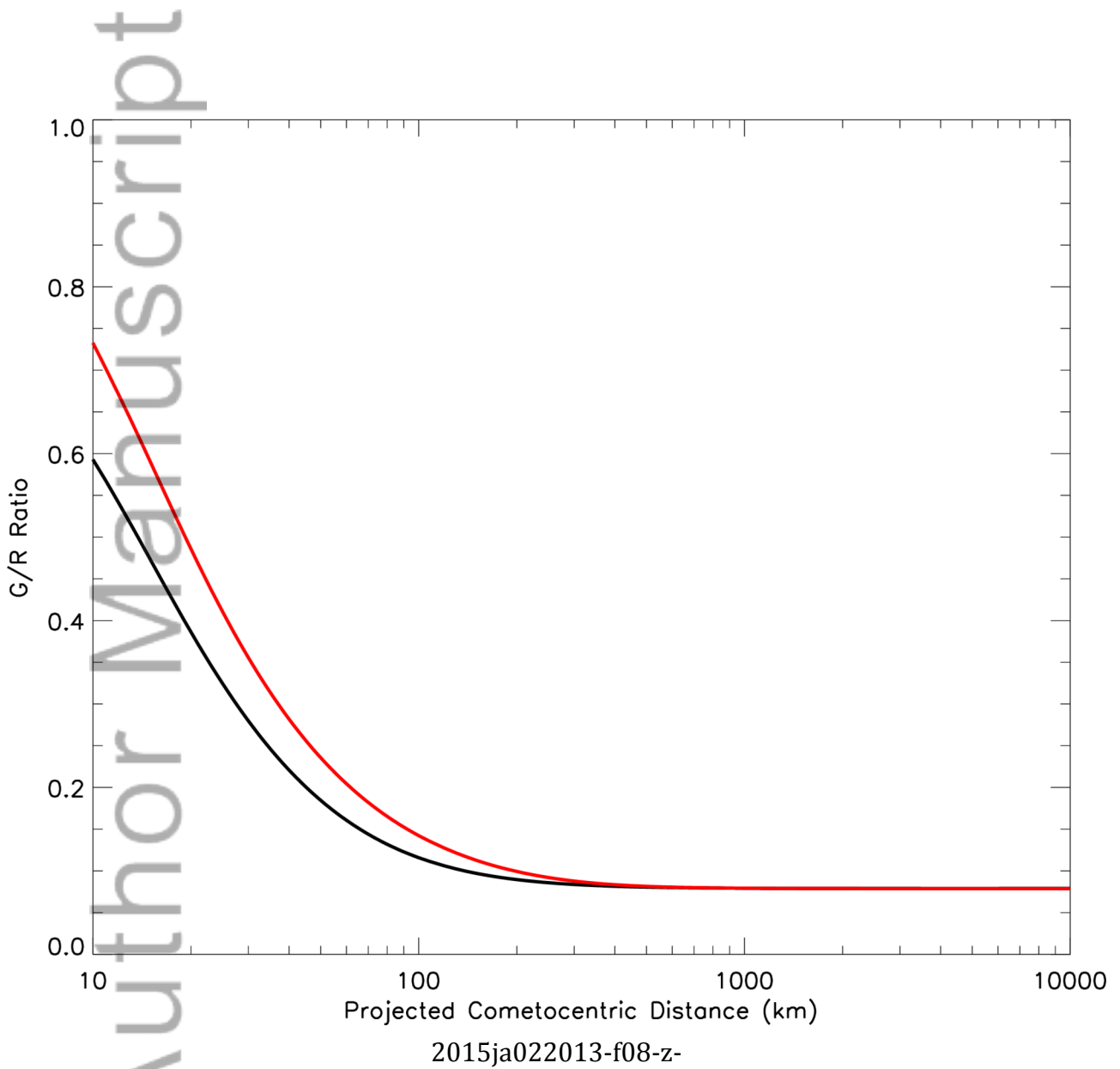
2015ja022013-f04-z-

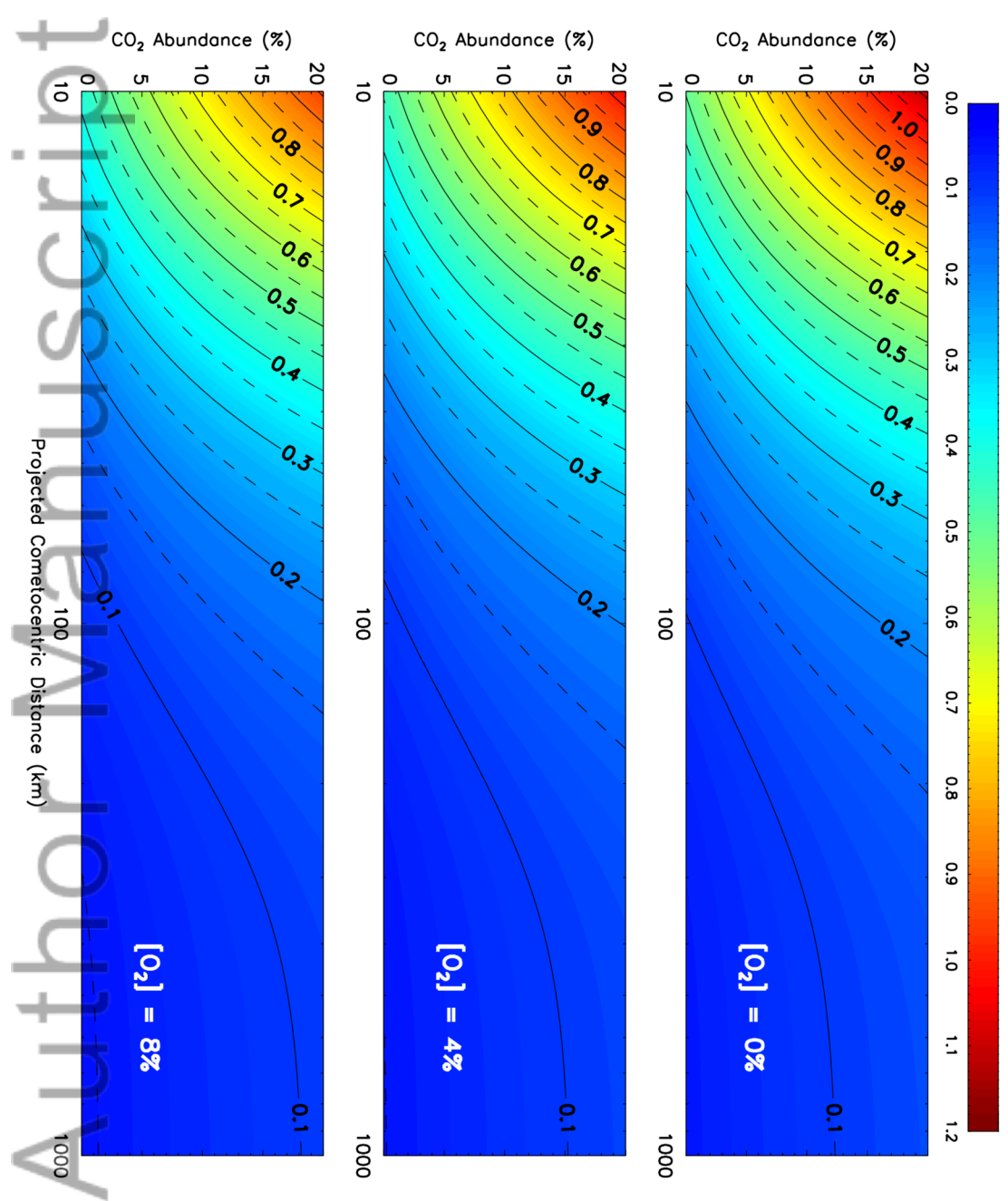












2015ja022013-f09-z-